Desalination 544 (2022) 116128

Contents lists available at ScienceDirect

Desalination

journal homepage: www.elsevier.com/locate/desal

Determining the operational window of green antiscalants: A case study for calcium sulfate

P. Ramírez-García [a], M.A. Durán-Olivencia [b,c], M. Kellermeier [d], A.E.S. Van Driessche [a,*]

[a] Instituto Andaluz de Ciencias de la Tierra (IACT), CSIC-University of Granada, 18100 Armilla, Granada, Spain
[b] Institute for Research in Technology (IIT), ICAI School of Engineering, Universidad Pontificia Comillas, C/Santa Cruz de Marcenado 26, Madrid, Spain
[c] Complex Multiscale Systems Group - Department of Chemical Engineering, Imperial College London, London, UK
[d] BASF SE, Material Science, RGA/BM - B007, 67056 Ludwigshafen am Rhein, Germany

HIGHLIGHTS

- High-throughput method to benchmark scaling kinetics and test the performance scale-inhibitors
- Evaluation of the antiscaling potential of green additives under different application conditions
- Performance of chelating agent and a threshold inhibitor in delaying $CaSO_4$ precipitation
- Direct route to a more rational design of antiscaling technologies

ARTICLE INFO

Keywords:
Antiscaling
Chelating agents
Threshold inhibitors
Nucleation induction times
Calcium sulfate
Polycarboxylates

ABSTRACT

The detrimental effects of inorganic scaling in industrial and domestic applications are often mitigated with scale inhibitors. Increasing environmental awareness and stringent regulations require developing more sustainable antiscalants. Testing of suitable candidates is often the rate-limiting step in development cycles, therefore we developed a high-throughput methodology to rapidly evaluate the antiscaling potential of new additives under different application conditions. Using this method we determined the performance of two potential green additives – a chelating agent and a threshold inhibitor – in delaying $CaSO_4$ precipitation over a wide range of supersaturations, temperatures and salinities. The threshold inhibitor strongly delayed $CaSO_4$ scaling, but its performance is highly dependent on the physicochemical conditions, with the appropriate application window comprising low salinities and mild temperatures. In contrast, the chelating agent showed a lower inhibiting capacity, but its performance remained relatively constant throughout the entire matrix of physicochemical conditions. Noteworthy, we also observed that at intermediate salinities the absolute induction time for $CaSO_4$ precipitation is dramatically prolonged, offering a sustainable strategy to mitigate scaling. Overall, our method allows simultaneously benchmarking the scaling kinetics and testing the scale-inhibiting performance of additives, providing a direct route to a more rational design of antiscaling technologies.

1. Introduction

Inorganic scaling is a major issue in many industrial and domestic applications and involves the precipitation of metal carbonates, sulfates, oxides and hydroxides from solution induced by temperature changes, evaporation or pressure decrease [1]. These incrustations usually form at heat exchanger surfaces, inside pipes, and on membranes during distillation (MD) or reverse osmosis (RO), drastically reducing the efficiency of desalination units [2–4], heat exchangers [5], and facilities for oil and gas recovery [6,7]. Feed water (pre)treatment is routinely used to mitigate scale formation in water-intensive systems such as desalination units or home care appliances [3,7,8], including: (a) pH adjustment of the solution, (b) use of ion exchangers to remove scale-forming ("hardness") ions like Ca^{2+} or Mg^{2+}, (c) addition of chelating agents, or sequestrants, causing a decrease of the effective supersaturation due to complexation of the scale-forming ions, and/or (d) addition of small amounts of water-soluble additives that actively suppress scale formation. While the first approach is very effective in avoiding carbonate

* Corresponding author.
E-mail address: alexander.vd@csic.es (A.E.S. Van Driessche).

https://doi.org/10.1016/j.desal.2022.116128
Received 9 June 2022; Received in revised form 15 September 2022; Accepted 18 September 2022
Available online 7 October 2022

scales, it fails to control for example sulfate scales due to the weak pH dependence of the solubility of these minerals; moreover, low pH tends to accelerate corrosion and is detrimental for boron elimination from seawater. The second method can reduce, or fully eliminate, scale formation but requires the regeneration of the ion exchange resins, which may increase the operational costs considerably. In the case of hardness ion sequestration (third approach), relatively high concentrations of chelating agents (usually matching those of the cations in case of 1:1 complexes) are needed to effectively suppress scaling, which results in both higher operating costs and a larger environmental impact [7,8]. The last, and often the most cost-effective, approach involves the addition of sub-stoichiometric amounts (typically in the ppm range) of water-soluble additives to the process water [9]. These so-called "threshold inhibitors" fall into two categories: (i) non-polymeric (in) organic species such as magnesium, pyrophosphate, or phosphonates ions, and (ii) polymeric compounds like polycarboxylates, polyphosphates, polyphosphonates and copolymers containing monomers with different additional functional groups (e.g. sulfonates). These additives are primarily developed to delay crystal nucleation and/or growth by interacting with cations and/or anions constituting the minerals, present either on their surfaces or dissolved in solution. Further effects of such inhibitors may also include modifications of the crystal habit, which for example reduces their propensity to adhere to equipment surfaces or block membranes [1].

Unfortunately, most high performance antiscaling agents are (intentionally or unintentionally) are not readily biodegradable (e.g. polymers with acrylic backbones) and, as a consequence, they usually persist for many years after their disposal in the environment. In addition, phosphorus-based inhibitors are of particular concern because they can serve as nutrients to organisms and thus cause eutrophication (e.g. [10]). Increased environmental awareness, as well as discharge limitations, has encouraged both industrial and academic researchers to develop antiscalants that readily biodegrade and have low molecular mobility to reduce their environmental impact [11–13]. However, the design and subsequent synthesis of any such new classes of "green" additives with acceptable levels of performance and cost-effective dose-response profiles can be a daunting and time-consuming task. One crucial, and often limiting step in typical development cycles is to test the performance of the newly synthesized scale inhibitors across a wide range of relevant operational conditions, including ionic strength, pH, temperature, pressure, hydrodynamic regimes, and/or scaling mechanisms (i.e. surface-induced versus homogeneous). Although a suite of approaches exists to test the performance of antiscalants, most of these methods are rather tedious and only assess a limited matrix of physicochemical parameters (focusing solely one a specific application, e.g. only for RO), let alone their combination with other potential ingredients in more complex antiscalant formulations [14–16]. Hence, there is a need for high-throughput tools to evaluate the scaling potential of different mineral phases and to determine the corresponding universal (i.e. across multiple applications) operational window of new antiscalants, in order to provide profound assessment of their performance and thus enable rational selection of promising candidates on the way from the laboratory to the industry.

To this end, we have designed a high-throughput approach that relies on a standard time-resolved UV/Vis spectrophotometer and automated data analysis. This benchtop method provides quantitative information on the progress of mineral precipitation reactions and the delaying capacity of added antiscalants, from which their respective optimal operational window can be extracted in a straightforward manner. To illustrate the usefulness of this approach, we have evaluated the performance of two types of potential "green" scale inhibitors, namely poly ((methyl vinyl ether-*alt*-maleic acid) (PM) and gluconic acid (GA), in preventing mineral precipitation in the $CaSO_4$-NaCl-H_2O system. We used this mineral system for a first case study because (i) calcium sulfate scales (i.e. gypsum, bassanite or anhydrite) are one of the most commonly encountered incrustations in e.g. desalination units over a wide range of operational conditions [2,3,8,17–19], and (ii) their solubility is pH-independent and as such, $CaSO_4$-based scales cannot be removed by acid cleaning procedures. Thus, the only effective strategy to mitigate calcium sulfate scaling is through the addition of chelators and/or threshold inhibitors during the water (pre-)treatment stages. We selected PM and GA as additives to be tested because (i) they represent two types of antiscalants, i.e. a threshold inhibitor and a chelator, and (ii) these molecules have not yet been extensively tested as additives for scale prevention. Hence, this allows us to test the ability of our method to quantify, and compare, the inhibitory effects of potential alternative (and ideally more sustainable) antiscalants. To establish a comprehensive picture, we first evaluated the $CaSO_4$ scaling potential and then determined the antiscaling performance of both additives as a function of solution salinity (ionic strength), temperature and supersaturation, in order to delineate their optimal operational windows.

2. Materials and methods

2.1. "Green" scale inhibitors

At present no consensus definition of the term "green inhibitor" exists in the literature (i.e. legislation) and the requirement for any such classification will depend strongly on the region/country in question. In general terms, a scale inhibitor can be considered as environmentally benign when the following criteria are met (e.g. [20,21]): (1) excellent (or at least acceptable) scale inhibition performance, (2) low to very low mammalian toxicity, (3) low water hazard class (usually linked to biodegradability, low bioaccumulation potential and low aquatic toxicity), and (4) chemistry free of phosphorus, nitrogen and heavy metals. Regarding the additives used for this study (see Table 1), D-gluconic acid is a well-known sustainable additive meeting all criteria mentioned above. In the case of PM, specific information about biodegradability, bioaccumulation and aquatic toxicity is not available at the moment; however, this polymer qualifies as highly biocompatible, biodegradable and is routinely used for drug delivery and other biomedical applications (e.g. [22–24]).

Both poly(methyl vinyl ether-*alt*-maleic acid) (PM) and D-gluconic acid (GA) were obtained from Sigma-Aldrich. Their chemical formula, structure, molecular weight (MW), and biological impact profile (for GA) are summarized in Table 1. Stock solutions of each additive were prepared by dissolving PM and GA, respectively, in deionized water (18.2 mΩ cm^{-1}) and subsequent filtration through 0.22 μm membranes.

Table 1
Characteristics of the antiscaling agents used in this study. $logP_{ow}$ stands for the octanol/water partition coefficient, LC_0 the maximum concentration causing no mortality, and LD_{50} the lethal dose causing 50 % of mortality.

Additive	Poly(methyl vinyl ether-*alt*-maleic acid)	D-Gluconic acid
Acronym	PM	GA
Formula	$[CH_2CH(OCH_3)CH(CO_2H)CH(CO_2H)]_n$	$C_6H_{12}O_7$
Structure	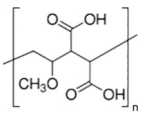	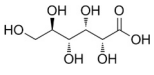
MW (g mol^{-1})	216,000	196
Biodegradation	n/a	98 % after 48 h[b]
Bioaccumulation	n/a	$logP_{OW}$ −1.87[c]
Aquatic toxicity	n/a	LC_0 > 100 mg/L
Mammalian toxicity (acute oral toxicity)	LD_{50} (rat) >5000 mg/kg[a]	n/a

[a] [24].
[b] [25].
[c] [26].

2.2. Precipitation of calcium sulfate

Reagent grade chemicals and grade A glassware were used to prepare stock solutions of calcium chloride, sodium sulfate and sodium chloride by dissolving the desired amount of $CaCl_2{\cdot}2H_2O$, Na_2SO_4 and NaCl (>99 %, all received from Sigma-Aldrich) in deionized water (18.2 MΩ cm^{-1}). These stock solutions were filtered through 0.22 μm membranes and stored at the desired temperature prior to mixing.

Calcium sulfate precipitation experiments were carried out by adding a fixed volume of the Na_2SO_4 stock solution (e.g. 1 mL) to the same volume of $CaCl_2$ stock solution under continuous stirring. In all cases, equimolar solutions were mixed to obtain 2 mL aliquots with final $CaSO_4$ concentrations ranging between 0.03 and 0.15 M (see Table 2). These solution compositions were chosen to represent typical conditions found in seawater and brackish feed water [3,27,28], and to also cover higher concentrations (>0.13 M) that occur at later stages of MD or RO water recovery processes [3,4,27,29]. In experiments containing additives, a defined volume of a stock solution of inhibitor was added to the sodium sulfate solution prior to mixing with the calcium chloride solution, maintaining a constant final concentration of 5 ppm PM (equivalent to 23 μM; see the Supporting Information (SI) and Fig. S3 for details) at all studied conditions (cf. Table 2), while the amount of added GA was matched with the respective final Ca^{2+} concentration. All precipitation experiments were conducted at three different levels of background salinity (0.3, 2.0 and 5.0 M NaCl) and four different temperatures (20, 40, 60 and 80 °C) (cf. Table 2). The experiments at low concentration of NaCl (0.3 M) served as a benchmark to be able to quantify the impact of salinity on the nucleation kinetics of CaSO4 at higher background ionic strength.

2.3. Solution speciation

The saturation state (S) of the solution with respect to a given $CaSO_4$ phase is defined as the ratio of the actual activity products and the thermodynamic solubility product of the mineral phase (K_{sp}). For gypsum, the main phase to form under all studied conditions [30,31], except 80 °C and 5 M NaCl, the precipitation reaction can be written as follows:

$$Ca^{2+} + SO_4^{2-} + 2H_2O \leftrightarrow CaSO_4{\cdot}2H_2O \quad (1)$$

at 80 °C and 5 M NaCl bassanite is forming and can be written as follows:

$$Ca^{2+} + SO_4^{2-} + 1/2H_2O \leftrightarrow CaSO_4{\cdot}1/2H_2O \quad (2)$$

The saturation index is defined as the decadic logarithm of the saturation state ($\log_{10}S$). The saturation index for each condition was calculated with the PHREEQC code, using the phreeqc and pitzer databases for low (0.3 M NaCl) and high salinity (2.0 and 5.0 M NaCl) solutions, respectively [32]. Protonation and complexation constants for the interaction of GA with Ca^{2+} ions were obtained from the Andra thermodynamic database [33].

Table 2
Experimental conditions chosen for studying calcium sulfate precipitation at varying final $CaSO_4$ concentrations, salinities and temperatures (resulting in different final supersaturation indices ($\log_{10}S$) with PM and GA as scale inhibitors.

$CaSO_4$ (M)	T (°C)	NaCl (M)	$\log_{10}S$ (−)	PM (M)	GA (M)
0.150	20 – 40 – 60 – 80	0.3 – 2.0 – 5.0	0.76–1.12	2.3×10^{-5}	0.150
0.140	20 – 40 – 60 – 80	0.3 – 2.0 – 5.0	0.71–1.08	2.3×10^{-5}	0.140
0.125	20 – 40 – 60 – 80	0.3 – 2.0 – 5.0	0.63–1.01	2.3×10^{-5}	0.125
0.100	20 – 40 – 60 – 80	0.3 – 2.0 – 5.0	0.46–0.87	2.3×10^{-5}	0.100
0.095	20 – 40 – 60 – 80	0.3 – 2.0 – 5.0	0.43–0.83	2.3×10^{-5}	0.095
0.085	20 – 40 – 60 – 80	0.3 – 2.0 – 5.0	0.34–0.76	2.3×10^{-5}	0.085
0.075	20 – 40 – 60 – 80	0.3 – 2.0 – 5.0	0.25–0.68	2.3×10^{-5}	0.075
0.065	20 – 40 – 60 – 80	0.3 – 2.0 – 5.0	0.14–0.59	2.3×10^{-5}	0.065
0.055	20 – 40 – 60 – 80	2.0 – 5.0	0.02–0.15	2.3×10^{-5}	0.055
0.050	20 – 40 – 60 – 80	0.3 – 2.0 – 5.0	0.00–0.41	2.3×10^{-5}	0.050
0.040	20 – 40 – 60 – 80	0.3	0.22–0.26	–	–
0.030	20 – 60	0.3	0.02–0.05	–	–

2.4. Determination of induction times

The most relevant experimental parameter to consider during inorganic scaling is the induction time, t_{ind}, which can be defined as the time elapsed between the onset of supersaturation and the formation of critical clusters, i.e. stable nuclei that subsequently grow (or transform) into crystals. In the case of precipitation from solution, this interval primarily depends on the saturation index and other physicochemical parameters of the solution such as temperature, hydrodynamic regime (e.g. stirring rate), presence of foreign particles, or viscosity. However, experimentally it is very challenging to capture the formation of the first nuclei. In order to be detected, these nuclei need to grow until they (i) reach an observable size, which will depend on the temporal and spatial resolution of the used technique, or (ii) induce a detectable change in the solution speciation, which will depend on the sensitivity of the used probes (e.g. immersed conductivity or ion-selective sensors). Consequently, the experimentally determined (apparent) induction period is usually the result of several separate contributions [34,35]: (1) a certain relaxation (or equilibration) time, t_{pnc}, required for the system to achieve a quasi-steady-state distribution of molecular clusters (e.g. the formation of pre-nucleation clusters); (2) the time elapsed until these molecular clusters have developed into nuclei, t_{nuc}; and (3) the time required for the nuclei to grow to a detectable size, t_{gr}. The measured induction time can therefore be expressed as:

$$t_{ind} = t_{pnc} + t_{nuc} + t_{gr} \quad (3)$$

At present it is still difficult, if not impossible, to isolate these separate quantities. The relaxation time, t_{pnc}, depends to a great extent on the viscosity of the medium and, hence, diffusivity. In solution, this process is assumed to be very fast (e.g. [36]), and should occur virtually instantaneously in the case of $CaSO_4$ [37,38]. The nucleation time, t_{nuc}, is mainly controlled by the solution supersaturation, and to a lesser extent by other physicochemical parameters such as temperature and salinity. Finally, the growth time, t_{gr}, depends on the size at which nuclei become detectable (i.e. the spatial resolution of the used detection method) and the growth rate applicable to this early stage of evolution. The latter contribution is difficult to estimate since the growth rate of a nucleus cannot be approximated by that of a macroscopic crystal, but in general it tends to be several orders of magnitude faster (e.g. [39]). Taking into account the sensitivity of currently available observation techniques, we can conclude that for sparsely soluble salts and the experimental conditions used in this work, the overall induction time will be dominated by the time required to form a stable nucleus, i.e. $t_{ind} \sim t_{nuc}$ [34–36,40].

Using the classical nucleation theory (CNT), analytical expressions for the nucleation time as a function of the supersaturation have been previously derived ([40] and references therein), allowing to extract characteristic kinetic and thermodynamic information of the nucleation process. Most of these models rely on the basic assumption that the initial formed nuclei have identical properties as the final macroscopic crystals (the so-called “capillary assumption” of CNT). However, extensive experimental and computational research during the past

decade has shown that for many sparsely soluble salts, this is not necessarily the case and more complex, so-called "non-classical", nucleation mechanisms involving multiple precursor and/or intermediate phases are at play [41]. In the case of $CaSO_4$, such a multistep pathway has been experimentally observed for both gypsum and bassanite nucleation, where the formation of the respective crystalline modification was found to be preceded by a disordered $CaSO_4$ phase [37,38,42]. For the purpose of the present work, we consider the measured induction times as being representative of the first detectable formation of phase-separated particles in solution, the nature of which is not necessarily equal to that of the final crystalline phase.

Induction times of calcium sulfate precipitation in the absence and presence of additives were determined by monitoring the change in transmittance of supersaturated solutions at different $CaSO_4$ concentrations, background salinities and temperatures (cf. Table 2). Changes in absorbance were monitored using time-resolved UV–Vis spectrophotometry performed on an Agilent Cary 300 instrument at acquisition times ranging from 1 to 6 s per data point. Measurements were carried out at a wavelength of 500 nm in disposable 3 mL polystyrene cuvettes, which were placed into multicell (6×) module that was temperature-controlled by means of a Peltier element (see Fig. S1 in the SI). During the induction time measurements, the supersaturated solutions were continuously stirred with magnetic stirrer bars (8 × 3 mm) in order to avoid gravitational setting of the formed solid phase(s). Measurements were repeated at least six times for each studied set of conditions and the results are given as average values with corresponding one-sigma standard deviations.

2.5. Automated data analysis

As discussed above, the time elapsed between the generation of a supersaturated solution and the first change in absorbance detected with UV/Vis spectrophotometry was taken as the induction time. This key parameter was determined automatically from the time-resolved absorbance curves using custom software written in R [43]. The first step was to minimize the inherent noise of the experimental absorbance curves by computing a smoothing spline function. From the first derivative of the resulting curve, t_{ind} was taken as the first time when the derivative reached a value >2 % of its overall maximum. This threshold was selected such that the corresponding derivative value was appreciably different from the background (theoretically zero), and used consistently for all analyzed curves.

The obtained induction time values were plotted as a function of supersaturation and fitted using the general nucleation rate equation provided by CNT [40]:

$$t_{ind} = \frac{1}{JV} = \frac{1}{aSlog(S)exp\left(-\frac{W_*}{k_BT}\right)} \tag{4}$$

$$W_* = \frac{b\gamma^3}{27(k_BT)^3 log^2(S)} \tag{5}$$

where J is the nucleation rate, V the solution volume, S is the saturation state, W_* the work to form a critical cluster, k_B the Boltzmann constant, T the temperature and a and b are parameters which contain information about the kinetic and thermodynamic properties of the forming solid phase. For the purpose of fitting the experimental induction times as a function of supersaturation, Eqs. (4) and (5) can be rewritten as (with $A = \log(a)$):

$$log(t_{ind}) = -A - log(S) - log(log(S)) + \frac{b\gamma^3}{27(k_BT)^3 log^2(S)} \tag{6}$$

with

$$X = \frac{1}{log^2(S)}, \mathrm{Y} = log(t_{ind}) \tag{7}$$

and $B = b\gamma^3/27(k_BT)^3$, we obtain:

$$Y(X) = A - X^{-1/2} + \frac{1}{2}log(X) + BX \tag{8}$$

This equation was employed to compute the fitting of t_{ind} as a function of S (to do so $\log_{10}S$ was converted to $\log S$), using a non-linear weighted least-squares method, where the weighting function was introduced to take into account the experimental errors. The fit uncertainties were calculated by applying the method for propagation of uncertainties in Eqs. (4)–(8). The fitted dependence of induction time on supersaturation was primarily used to automatically quantify the effects of additives on the nucleation of calcium sulfate under the various studied conditions. In addition, the fitting was also used to extract interfacial energies and kinetic parameters of the nucleation process of $CaSO_4$ in the absence and presence of additives.

2.6. Characterization of the final solid phases

Phase identification of the formed precipitates was performed by Raman spectroscopy and powder X-ray diffraction (PXRD). At the end of the reaction, the solid phase was isolated by vacuum filtration using a 0.22 μm membrane filter. Raman analyses were carried out with a confocal Raman microscope (LAbRAM HR, Horiba, Japan), equipped with a diode laser emitting at 532 nm and a CCD detector. The laser beam was focused onto the sample through a 50× objective. In this way, Raman intensities (in counts per second, cps) were measured as a function of incoming wavenumber at a resolution of <3 cm^{-1}. PXRD diffractograms were acquired using a PANalytical diffractometer (X'Pert Pro) equipped with Bragg-Brentano configuration, a PIXcel multichannel detector, programmable divergence slits, and a Cu anode providing $K_{\alpha1}$ and $K_{\alpha2}$ radiation. Patterns were collected from 5 to 80° (2θ) and analyzed with the XPowder software package [44], using the ICDD-PDF2 database.

The size and morphology of the formed solid particles were characterized using scanning electron microscopy (SEM). For this purpose, filters carrying the isolated calcium sulfate crystals were mounted on SEM stubs and sputter-coated with gold. Samples were examined using a Quanta 400 environmental scanning electron microscope operating at 20 kV.

3. Results and discussion

3.1. Precipitation of $CaSO_4$ as a function of concentration, temperature and salinity

In order to be able to evaluate the ability of an additive to delay the precipitation of calcium sulfate from solution, it is imperative to first characterize this process for a pure system without additives. To establish a comprehensive benchmark, induction times were determined for precipitation at final $CaSO_4$ concentrations of 0.03–0.15 M (all supersaturated with respect to gypsum) temperatures of 20, 40, 60 and 80 °C, and background salinities of 0.3, 2.0 and 5.0 M NaCl. In Fig. 1, the measured induction times are represented as a function of the initial calcium sulfate concentration in solution for the three studied salinities and four temperatures. These data immediately reveal that $CaSO_4$ precipitation is delayed at increased salinity (Fig. 1a), while higher temperatures result in lower induction times (Fig. 1b). The former trend is a direct consequence of the increased solubility of gypsum at higher salinity, as already reported in previous studies [45,46]. The retarding effect is more pronounced in solutions containing 2.0 M NaCl compared to 0.3 and 5.0 M NaCl (cf. Fig. 1a), in full agreement with reported gypsum solubility data as a function of salinity (Fig. 1c). The delaying

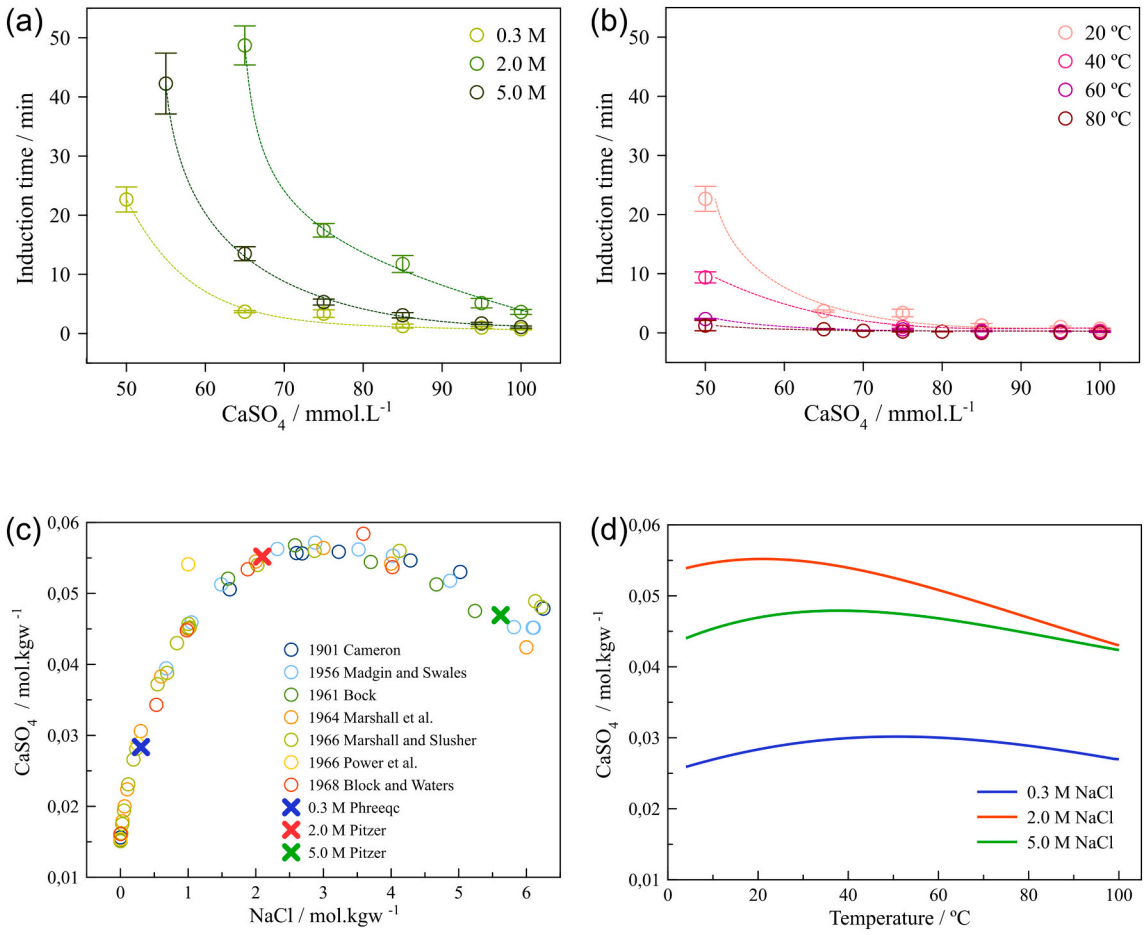

Fig. 1. Precipitation of calcium sulfate under various conditions in the absence of antiscaling additives. (a) Induction times as a function of $CaSO_4$ concentration at 0.3, 2.0 and 5.0 M NaCl and 20 °C. Note that at 0.3 M NaCl, the induction time for a 40 mM $CaSO_4$ solution is (854 ± 23) min, while for a 30 mM $CaSO_4$ solution no precipitation was observed after 6000 min. (b) Induction times as a function of $CaSO_4$ concentration at 20, 40, 60 and 80 °C at 0.3 M NaCl. (c) Solubility of gypsum as a function of salinity at 20 °C (adapted from [48] and references therein). Solubility values calculated for the experimental conditions studied in the present work are indicated as crosses. (d) Solubility of gypsum (calculated with PHREEQC) as a function of temperature at three different salinities.

effect of increased salinity is most significant at low $CaSO_4$ concentrations: for example, at 0.05 M $CaSO_4$ and 2.0 or 5.0 M NaCl, precipitation is completely inhibited for at least 700 min over the entire range of temperatures, while at 0.3 M NaCl nucleation already takes places after ~20 min (cf. Fig. 1a). On the other hand, the observed trend in induction times as a function of temperature at fixed salinity (cf. Fig. 1b) cannot be explained solely by taking into account temperature-dependent variations of gypsum solubility. For example, in the case of 0.3 M NaCl, the lowest solubility is expected at 20 °C (Fig. 1d), yet at higher temperatures the measured induction times are much shorter (cf. Fig. 1b). Hence, at a fixed salinity induction times appear to be controlled by faster reaction rates with increasing temperature, confirming previous observations [46,47].

The solid phase(s) present at the end of the precipitation reaction were identified by Raman spectroscopy. Under all studied experimental conditions, phase-pure gypsum was formed (see Fig. S2 in the SI) – except for precipitation at 80 °C and 5.0 M NaCl, where Raman spectra showed two main peaks at 435 and 1016 cm^{-1} (Fig. S1), indicating the presence of calcium sulfate hemihydrate (i.e. bassanite) along with minor amounts of gypsum (small peak at ~1138 cm^{-1}), which was most likely formed during isolation by vacuum filtration at room temperature. This preferred primary precipitation of bassanite at 80 °C and high salinity corroborates experimental results obtained in previous work [30,31]. At this point, it is important to note that based on thermodynamic arguments (i.e. solubility) only, anhydrite should be the main (i.e. stable) solid phase to form at temperatures above 50 ± 5 °C (e.g. [48]). Nevertheless, it is well known that up to 80 °C, gypsum is the only solid phase to precipitate, while high salinities (>3 M NaCl) favor the formation of bassanite [30,31]. Direct precipitation of anhydrite from solution indeed only occurs at temperatures above 120 °C (e.g. [30,49]). With time, initially formed gypsum and bassanite will convert to anhydrite at temperatures >(50 ± 5) °C in contact with an aqueous solution, but this process is very slow and may take >2 years [30]. This highlights that nucleation kinetics largely determines which calcium sulfate phase will precipitate under a given set of physicochemical solution conditions [30,31,42]. Consequently, it is of paramount importance to consider this aspect when developing effective antiscaling strategies.

3.2. *Kinetics of calcium sulfate nucleation*

To uncover the intrinsic influence of ionic strength and temperature on the kinetics of $CaSO_4$ nucleation, the measured induction times need to be compared while taking into account the supersaturation with respect to the forming solid phase. Following the classical nucleation rate equation (cf. Eq. (6)), t_{ind} values were plotted as a function of nominal supersaturation for all experimental conditions investigated (Fig. 2). Fig. 2a shows the dependence of the induction time on supersaturation at four different temperatures and a fixed salinity of 0.3 M NaCl. It is obvious that higher temperatures lead to shorter induction times, which decreases as the temperature increases.

Similar behavior was observed in experiments conducted in the

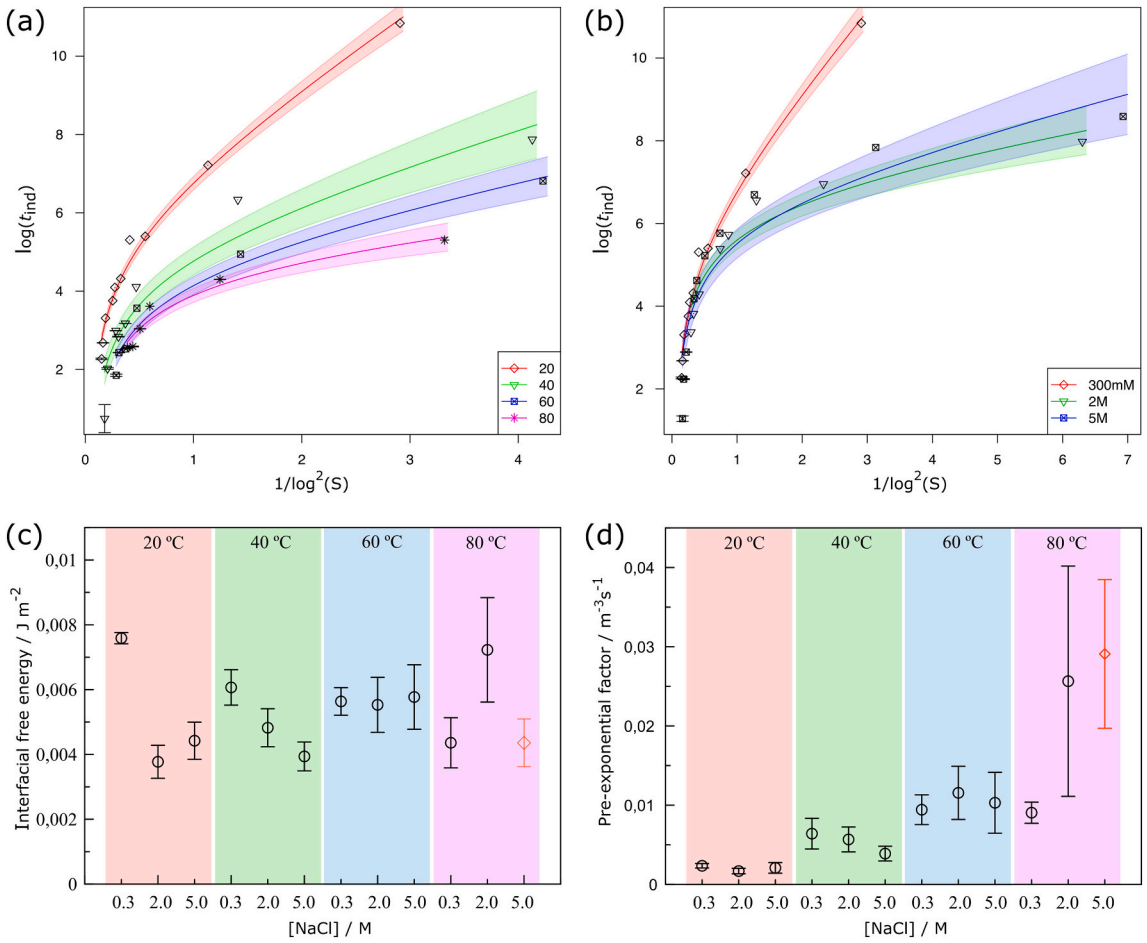

Fig. 2. Kinetics of calcium sulfate nucleation in the absence of additives. (a) Induction times as a function of supersaturation for different temperatures at 0.3 M NaCl. (b) Induction times as a function of supersaturation for different salinities at 20 °C. (c) Effective interfacial free energies and (d) pre-exponential factors *A* obtained by CNT-based analysis of the induction time data for the first formed solid phase. Red symbols indicate the conditions (5.0 M NaCl, 80 °C) where bassanite was obtained as main solid phase. Shaded areas in (a) and (b) represent one-sigma standard deviations.

presence of 2.0 and 5.0 M NaCl (see Fig. S4 in the SI). When induction times are plotted as a function of supersaturation at different background salinities (Fig. 2b), it becomes evident that the kinetics of calcium sulfate nucleation also depend strongly on the ionic strength of the solution. With increasing concentration of background electrolyte, the induction times are significantly reduced. Hence, $CaSO_4$ nucleation seems to be accelerated in the presence of NaCl – a finding confirmed by experiments performed at all other temperatures (see Fig. S5 in the SI).

Fitting the data shown in Fig. 2a and b using Eq. (6) yields the effective interfacial free energy (γ_{eff}) of the initially formed solid phase for the different temperatures and salinities investigated in this work. The results (Fig. 2c) indicate only a minor, if any, dependence of γ_{eff} on temperature and salinity. For example, at 20 and 40 °C γ_{eff} appears to decrease with increasing salinity. However, the relatively large error bars associated with γ_{eff} values and the uncertainty of $CaSO_4$ solubility (and thus nominal supersaturation) at high salinities and temperatures [48] call definite conclusions into question. This is also reflected in the existing literature, where apparently contradictory observations are reported about the dependence (or lack of dependence) of γ_{eff} on temperature and salinity (e.g. [45–47,49,50]). In any case, CNT does not predict any significant influence of temperature and salinity on the interfacial free energy [40]. To resolve this issue, induction times should be measured for a broader range of supersaturation and the solubility at high salinities and temperatures needs to be determined accurately. This will be subject of a forthcoming study.

While the role of the interfacial free energy in the rate equation of classical nucleation theory (Eq. (6)) is a frequently addressed topic, the pre-exponential kinetic factor, *A*, has received far less attention. Nevertheless, several studies have highlighted the relevance of this parameter for the resulting nucleation rate (e.g. [51,52]). In essence, the kinetic factor depends on the solute density of the liquid phase, the rate of attachment of atoms/ions/molecules to the critical cluster, and the Zeldovich factor, which describes the curvature of the free energy landscape at the top of the barrier. The lack of detailed analyses of the kinetic factor in previous studies is probably related to the fact that both the molecular attachment rate and the Zeldovich factor are difficult to determine experimentally. In Fig. 2d, the *A* values obtained from fitting the experimental data are plotted as a function of salinity and temperature, showing that temperature has a non-negligible effect on the pre-exponential factor. Typically, *A* increases with temperature– fully in line with the trends observed for the induction times as a function of the two parameters (cf. Fig. 1). Nonetheless, as already mentioned above, a more precise determination of γ_{eff} and *A* as a function of the physicochemical solution conditions is needed for a profound account of the relative importance of both parameters.

3.3. *Kinetics of calcium sulfate nucleation in the presence of "green" antiscalants*

To determine the operational window of the selected green scale inhibitors, series of precipitation experiments were carried out using the same experimental conditions as for the pure system, but adding a fixed

amount of 5 ppm PM and GA concentrations equimolar to calcium. Exemplarily, Fig. 3 shows induction times measured at 20 °C/0.3 M NaCl and 60 °C/2 M NaCl in the absence and presence of additives. As expected, the induction times for $CaSO_4$ precipitation were prolonged under the influence of PM and GA at all investigated experimental conditions. In particular, strong delay of nucleation was observed at low supersaturations and in the presence of PM. In the case of the complexing agent GA, the difference in induction time to the reference experiment without additive is less pronounced and remains approximately constant over the entire supersaturation range studied (despite the higher molar concentrations of GA used, as compared to PM).

The data shown in Fig. 4 already provides direct insight on the antiscaling performance of the two additives as a function of the physicochemical solution conditions. However, to better illustrate how salinity and temperature affect the ability of PM and GA to inhibit $CaSO_4$ precipitation, we chose to plot the ratio of the logarithmic induction times determined in the presence of additive and for the pure system as a function of supersaturation. This analysis was done for both additives at all temperatures and salinities probed in this study, yielding the results shown for PM and GA in Figs. 4 and 5, respectively.

From the profiles in Fig. 4, several important aspects of the antiscaling potential of PM at different solution conditions can be extracted: (i) at low to medium salinity (black and red traces in Fig. 4), PM is an effective inhibitor below a certain threshold supersaturation; (ii) at high salinity (green traces in Fig. 4), PM does not inhibit gypsum precipitation noticeably; (iii) within the observed operational window, PM is most effective at low salinity; (iv) up to 60 °C temperature does not significantly influence the antiscaling potential of PM, although at 2 M NaCl there appears a maximum in the antiscaling potential at 40 °C. Equivalently, the main antiscaling characteristics of GA can be directly inferred from Fig. 5: (i) for the studied conditions GA is not a strong inhibitor of $CaSO_4$ precipitation; (ii) its antiscaling potential is more or less independent of supersaturation; iii) at high salinity and medium temperatures, the antiscaling potential is slightly increased (green traces in Fig. 5b and c).

3.4. Inhibition mechanisms of PM and GA

The results presented above show that a trace quantity of PM markedly delays the precipitation of calcium sulfate in both low- and medium- saline solutions, whereas equimolar amounts of GA have a rather limited impact on the scaling behavior. The influence of antiscaling additives on the precipitation of inorganic minerals is traditionally explained by three mechanisms (e.g. [1,3,7,8]): (i) complexation with crystal lattice ions by additive molecules in solution; (ii) adsorption of the additive on the surface of nucleated particles; and/or (iii) changes in ionic strength of the medium and related variations of the solubility of the precipitating phase caused by the presence of the additive. The range of experimental conditions explored in this study allows us to consider and discuss all of these three potential mechanisms.

In the case of GA, which is a well-known complexing agent of Ca^{2+}

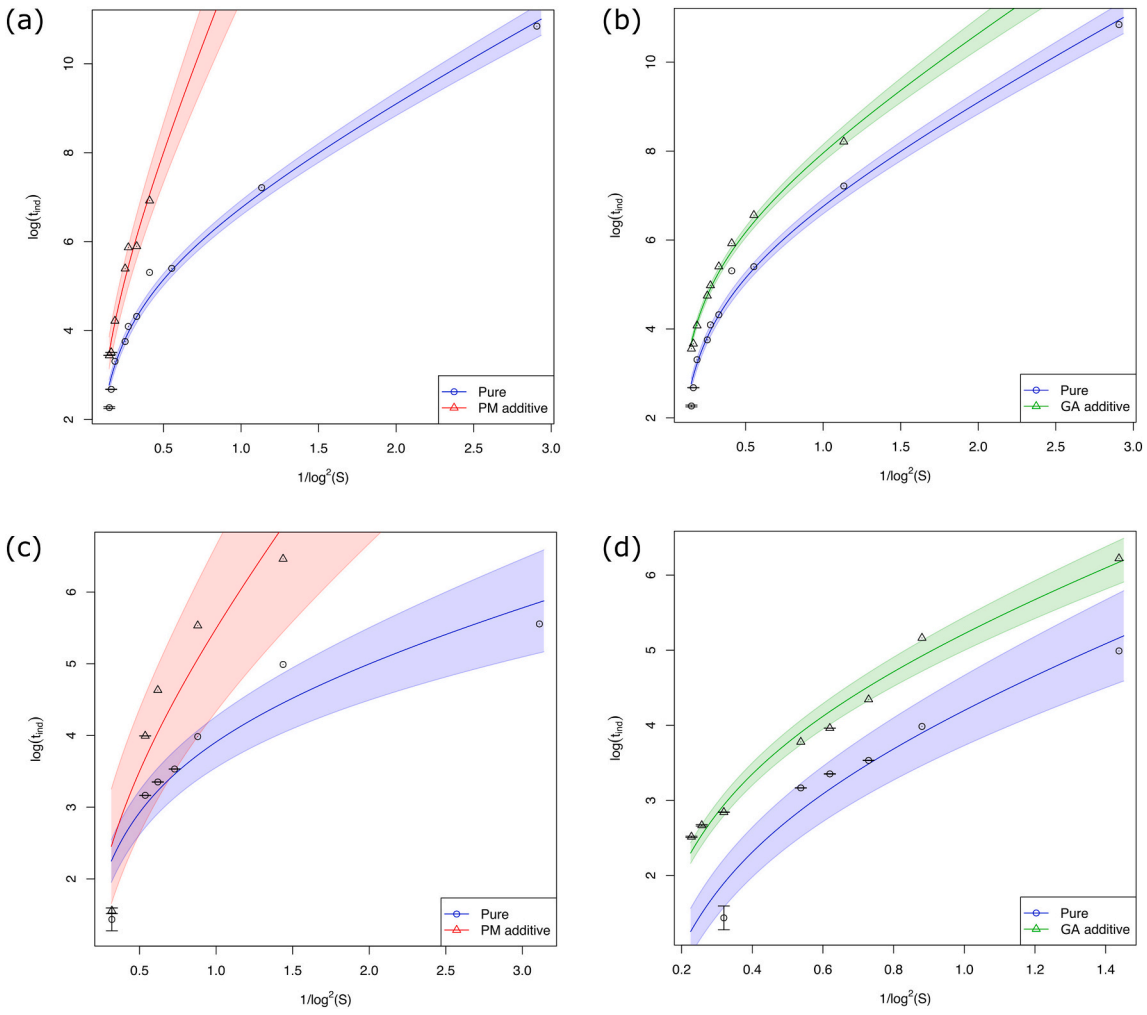

Fig. 3. Induction times as a function of supersaturation in the absence (blue) and presence of (a,c) 5 ppm PM (red) and (b,d) equimolar concentrations of Ca^{2+} and GA (green) at 20 °C and 0.3 M NaCl (a,b) or 60 °C and 2.0 M NaCl (c,d). Shaded areas represent one-sigma standard deviations.

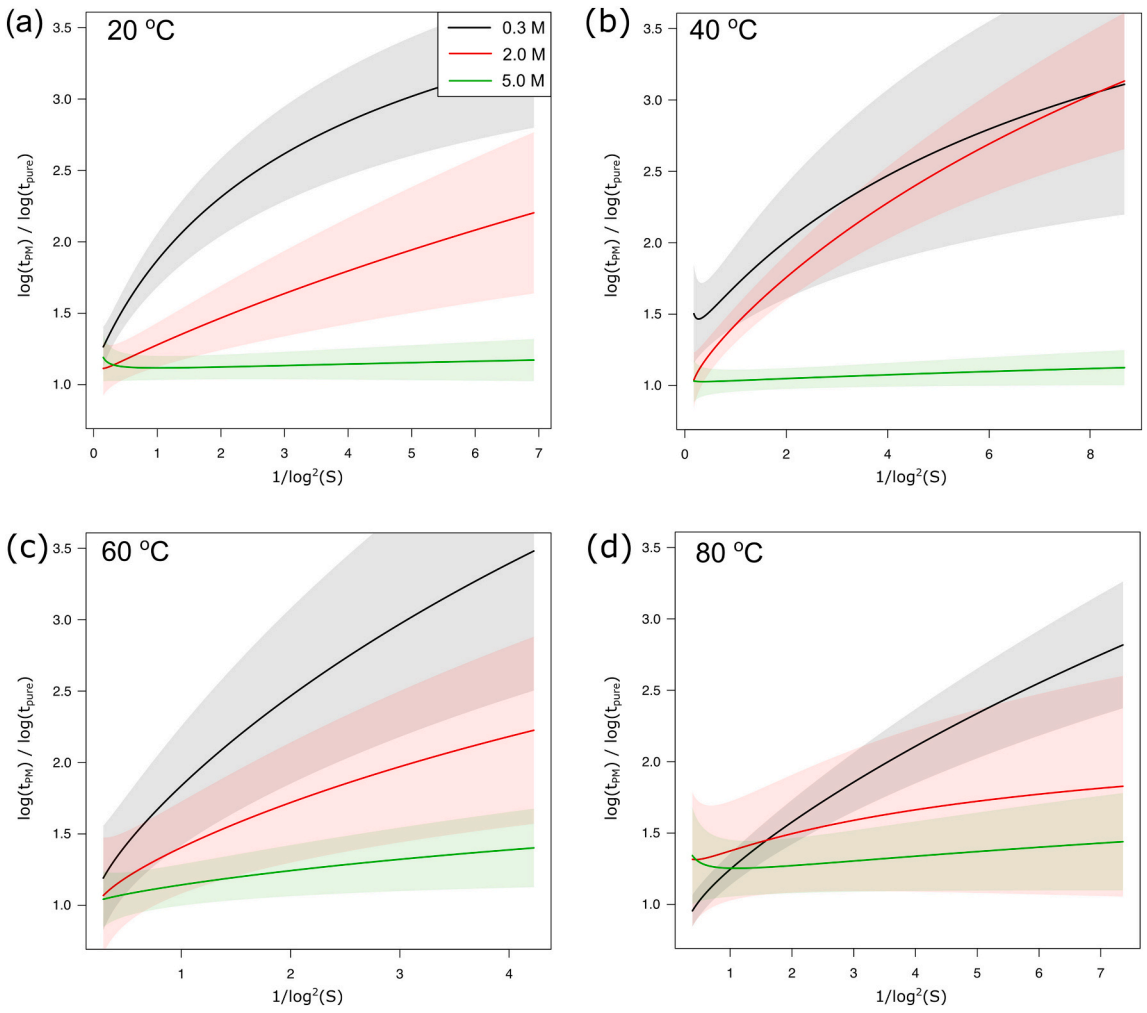

Fig. 4. Ratios of the logarithmic induction times measured for $CaSO_4$ precipitation in the presence and absence of PM as a function of supersaturation at (a) 20 °C, (b) 40 °C, (c) 60 °C and (d) 80 °C. Shaded areas represent one-sigma standard deviations.

(e.g. [53]), we observed a small – yet still significant – retarding effect on the precipitation of gypsum, as shown in Fig. 5. However, recalculation of these plots using the effective supersaturation, i.e. accounting for the Ca^{2+} ions sequestrated by GA (Figs. 6 and S6; calculated using PHREEQC) reveals that for the experimental conditions used in this study, the retarding effect can be entirely ascribed to the Ca^{2+} complexation. Hence, it seems safe to conclude that GA does not interfere directly with the nucleation pathway of calcium sulfate, i.e. neither the pre-exponential factor nor the effective interfacial free energy is affected by the presence of GA.

With PM as antiscaling agent, complexation can in turn not be responsible for the observed inhibiting effect on gypsum precipitation, since calculations with PHREEQC indicate that only a marginal fraction ($\ll$0.1 %) of the free Ca^{2+} ions is bound by PM. Due to the low concentration of additive used ($2.3 \cdot 10^{-8}$ M), the ionic strength of the solution will likewise also not be significantly changed. Thus, following the traditional view on the mechanisms of threshold inhibitors, adsorption on the surface of forming nuclei remains as key interaction to account for the inhibiting effect of PM. To obtain experimental support for the surface adsorption mechanism, the morphology of gypsum crystals precipitated in the presence of PM at low and high salinity was characterized using SEM (Fig. 7). In the absence of the additive, typical needle- and plate-shaped morphologies of gypsum were formed (Fig. 7a, b). Addition of $2.3 \cdot 10^{-8}$ M (5 ppm) PM does not induce noticeable morphological changes (Fig. 7c,d). However, the influence of PM on the growth behavior of gypsum crystals becomes evident at significantly higher additive concentrations, 0.93×10^{-7} M 200 ppm), where bulky crystals with jigsaw-like edges are obtained (Fig. 7e,f). Importantly, this habit modification, arguably induced by adsorption of PM on the growing crystal surfaces, occurs both at low (0.3 M) and high (5.0 M) background salinity. This stands in contrast with the nucleation inhibition potential of PM as a function of salinity, which decreases markedly with increasing NaCl concentration (cf. Fig. 4).

To gain additional insight into the possible inhibition mechanism of PM, we have extracted the pre-exponential factor and the effective interfacial free energy through fitting the dependence of induction times on supersaturation using Eq. (8) (see Fig. S8 in the SI). The results show that pre-exponential factor does not change significantly in the presence of PM (Fig. S8a), while γ_{eff} increases significantly at low and medium salinity (Fig. S8b). Hence, PM does not alter the kinetics of the nucleation process (e.g. by reducing the attachment rate of the ions/primary particles to the initial $CaSO_4$ clusters/nuclei [35,36,40]), but rather changes the thermodynamics of the nucleation process (e.g. by increasing the interfacial energy of the critical cluster). Commonly, it is assumed that such effects are caused by adsorption of additive molecules on the forming nuclei [50, and references therein]. This, however, is in apparent conflict with the observed increase in effective interfacial energy (cf. Fig. S8), as adsorption should actually lead to (and, among others, be driven by) a lowering of the total interfacial free energy [52,54]. Moreover, additive adsorption alone can also not account for the observed decrease in the inhibiting potential at high salinity (cf. Fig. 4), while the ability of the additive to alter the morphology of

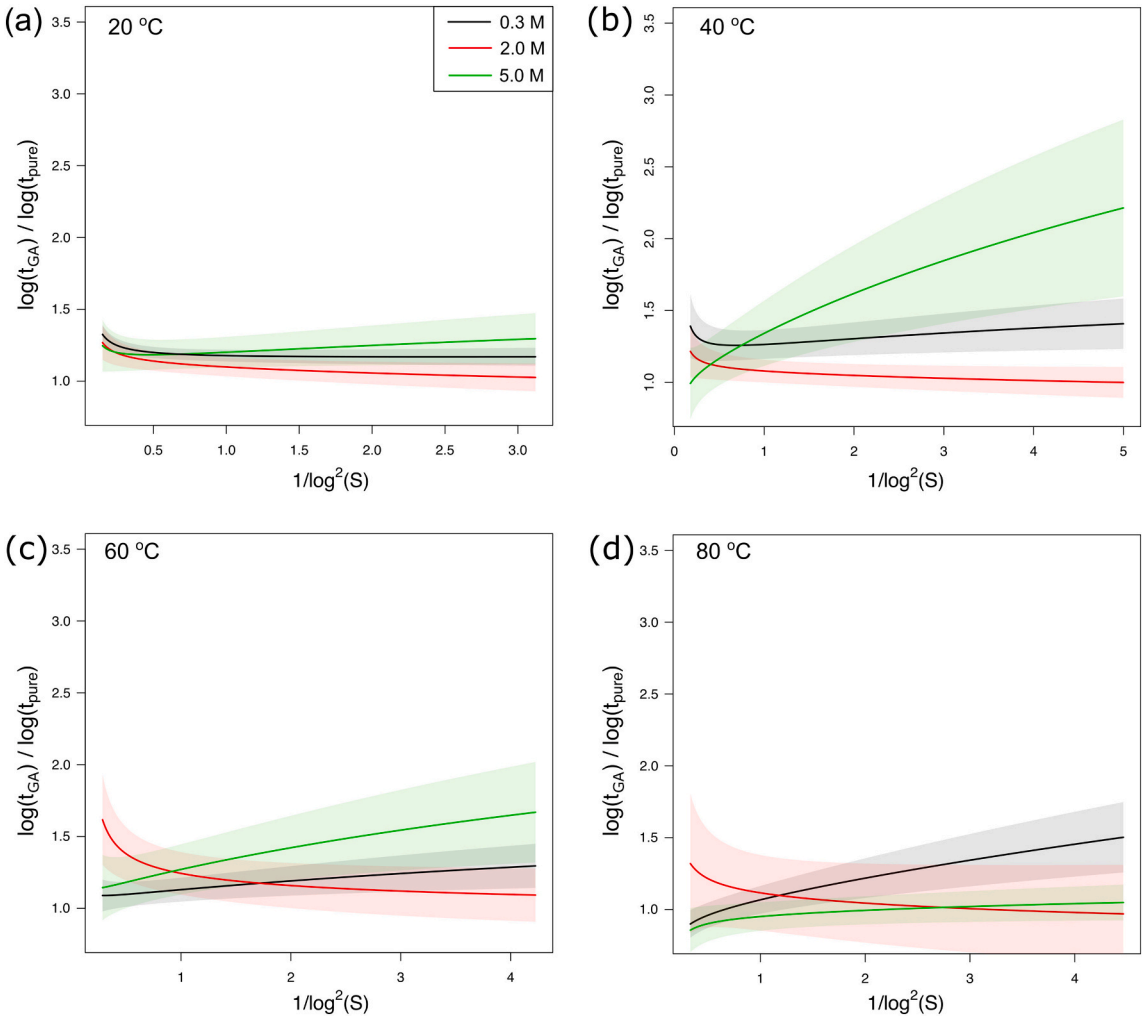

Fig. 5. Ratios of the logarithmic induction times measured for $CaSO_4$ precipitation in the presence and absence of GA as a function of supersaturation at (a) 20 °C, (b) 40 °C, (c) 60 °C and (d) 80 °C. Shaded areas represent one-sigma standard deviations.

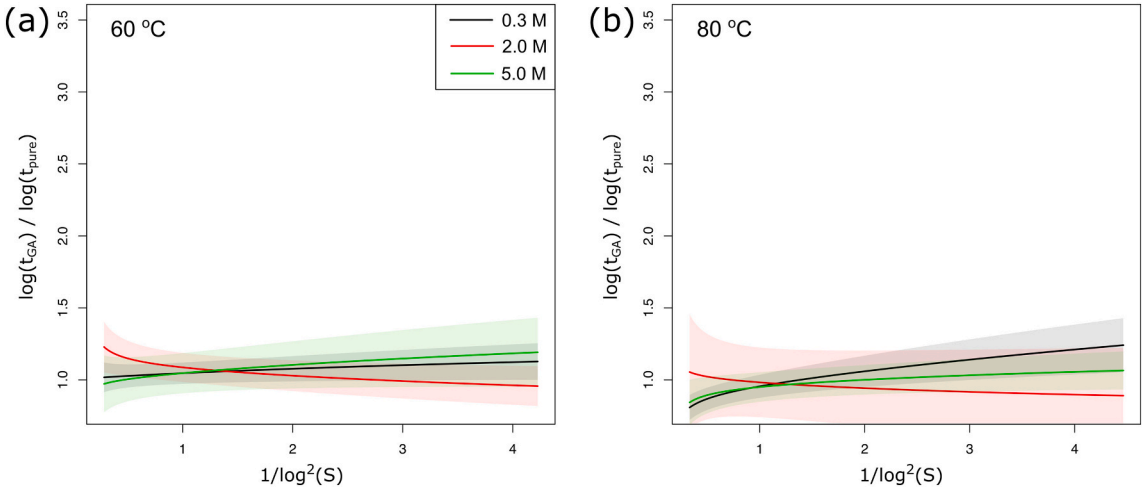

Fig. 6. Ratios of the logarithmic induction times measured for $CaSO_4$ precipitation in the presence and absence of GA as a function of the effective supersaturation (calculated taking into account complexation of calcium ions by GA) at (a) 60 °C and (b) 80 °C. Shaded areas represent one-sigma standard deviations. See Fig. S7 in the SI for corresponding plots at 20 and 40 °C.

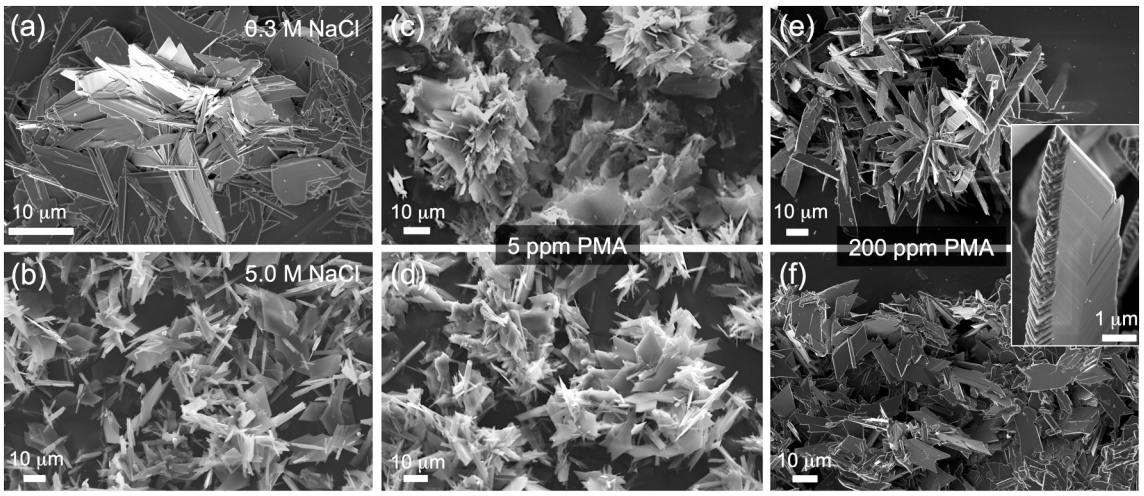

Fig. 7. SEM images of gypsum precipitated from 150 mM $CaSO_4$ solutions at 20 °C in the absence (a,b) and presence of 5 ppm (c,d) and 200 ppm (e,f) PM at 0.3 M (a, c,e) and 5.0 M (b,d,f) NaCl.

gypsum is retained under the same conditions (cf. Fig. 7). Possibly, PM changes the thermodynamics of gypsum nucleation through modulating the interaction potentials between the building blocks (ions and/or primary particles) of the nuclei [55]. This scenario could also explain the observed dependency of inhibition power on salinity (i.e. the loss of inhibition at 5.0 M NaCl, cf. Fig. 4): with increasing ionic strength, the charge of the carboxylate groups on the polymeric additives will be progressively screened, thus reducing any potential electrostatic interactions with ions, primary particles and/or clusters (whose interfacial charges will likewise be screened by the high salinity). Another potential mechanism behind the loss of performance at high salinity is salting out of the polymer, i.e. the intramolecular repulsion of the polymer chains is switched off and the polymer becomes partially insoluble. However, any such considerations are speculative at present and additional detailed experimental work is required to confirm or refute the hypothesis.

Comparing the molecular structures of the two chosen additives (cf. Table 1), it is evident that both potential antiscalants carry carboxylate groups, which are known to facilitate interactions with calcium ions in solution, calcium-terminated faces of crystalline particles as well as any of the precursors occurring on the way from dissolved ions to solid crystals (e.g. nanoclusters or amorphous phases). Any such interactions will likely be supported by further coordination of calcium ions to the hydroxy groups present in GA and/or the ether moieties in PM, as reported for complexes of calcium and alkylether carboxylates [56]. The main difference between the two additives is obviously their molecular weight, with the polymeric character of PM enabling multidentate binding to calcium-bearing interfaces, which allows the additive to become active and effectively inhibit nucleation already at low dosages (threshold effect). The affinity of PM towards the relevant interfaces might further be driven by the inherent hydrophobicity of its polyolefin backbone. GA, on the other hand, lacks the ability to incur cooperative binding processes and will therefore mainly act as a complexant for calcium ions (chelator effect), although molecular adsorption on calcium sulfate surfaces and related modulations of specific growth rates cannot be excluded.

3.5. Absolute delay of gypsum precipitation by PM and GA

Finally, we also consider the absolute delay in gypsum precipitation as a function of the physicochemical solution conditions, as a straightforward parameter that can more directly be related to real-world applications such as desalination by reverse osmosis or membrane distillation. In these settings, the residence time of the feed water and its concentrate(s) is the decisive factor determining whether scaling will occur or not. More specifically, mineral nucleation and scaling are expected to take place when the residence time exceeds the induction time. The main variables influencing the time window for effective inhibition of calcium sulfate scaling considered in this work were solute and background salt concentrations, operating temperature and type of antiscalant. However, it is important to note that in actual applied settings, other operational factors such as hydrodynamics, pressure and pH of the medium can also be relevant.

Fig. 8 shows a summary of the absolute induction times measured for calcium sulfate precipitation at different temperatures (20, 40, 60 and 80 °C), $CaSO_4$ concentrations (0.050 and 0.075 M) and NaCl contents (0.3, 2.0 and 5.0 M). These plots reveal that in the presence of 2.0 M NaCl at 0.050 M $CaSO_4$ (Fig. 8a), the formation of gypsum is greatly delayed (≥400 min) at all temperatures. This inhibition potential is somewhat reduced at 0.075 M $CaSO_4$ (Fig. 8b). At both calcium sulfate concentrations and all three levels of salinity, induction times increase with temperature. In the presence of additives, especially PM, calcium sulfate nucleation is further delayed but in fact, the inhibition potential of the additives strongly depends on background salinity (Fig. 8c,d): most notably, no precipitation was observed after 700 min with 5 ppm PM at 20 °C and a salinity of 2.0 M, while much shorter induction times were determined under the same conditions with 0.3 or 5.0 M NaCl (cf. Fig. 8c). This surprising finding suggests that background salinity could actually play an important role in controlling gypsum scaling but has to be adjusted properly for positive effects to occur. The most appropriate range of salinity will correspond to NaCl concentrations where gypsum solubility is maximized (i.e. 2.0–4.0 M NaCl, cf. Fig. 1c), while at the same time precipitation kinetics are not too fast (considering that nucleation kinetics are accelerated at higher background salinity, cf. Fig. 2b and d). In this regard, 2 M NaCl seems to be an optimal compromise between enhanced gypsum solubility and accelerated precipitation kinetics. Inhibition of calcium sulfate scaling is most effective at relatively low supersaturation, as illustrated by the different absolute induction times measured at 0.050 and 0.075 M $CaSO_4$ (cf. Fig. 8a vs. b). Upon addition of a potent antiscaling additive like PM, the salt-induced nucleation delay is maintained also at higher $CaSO_4$ concentrations. Hence, combining salinity with additives seems to offer a viable and cost-effective route to inhibit or completely prevent mineral precipitation under application-relevant conditions. This appears especially attractive when taking into account that high-salinity media are inherently produced during the desalination process. The only conditions where control over gypsum scaling remains challenging are found at higher temperatures (≥60 °C), due to a combination of accelerated nucleation kinetics (cf. Fig. 2a), decreased gypsum solubility (cf. Fig. 1d)

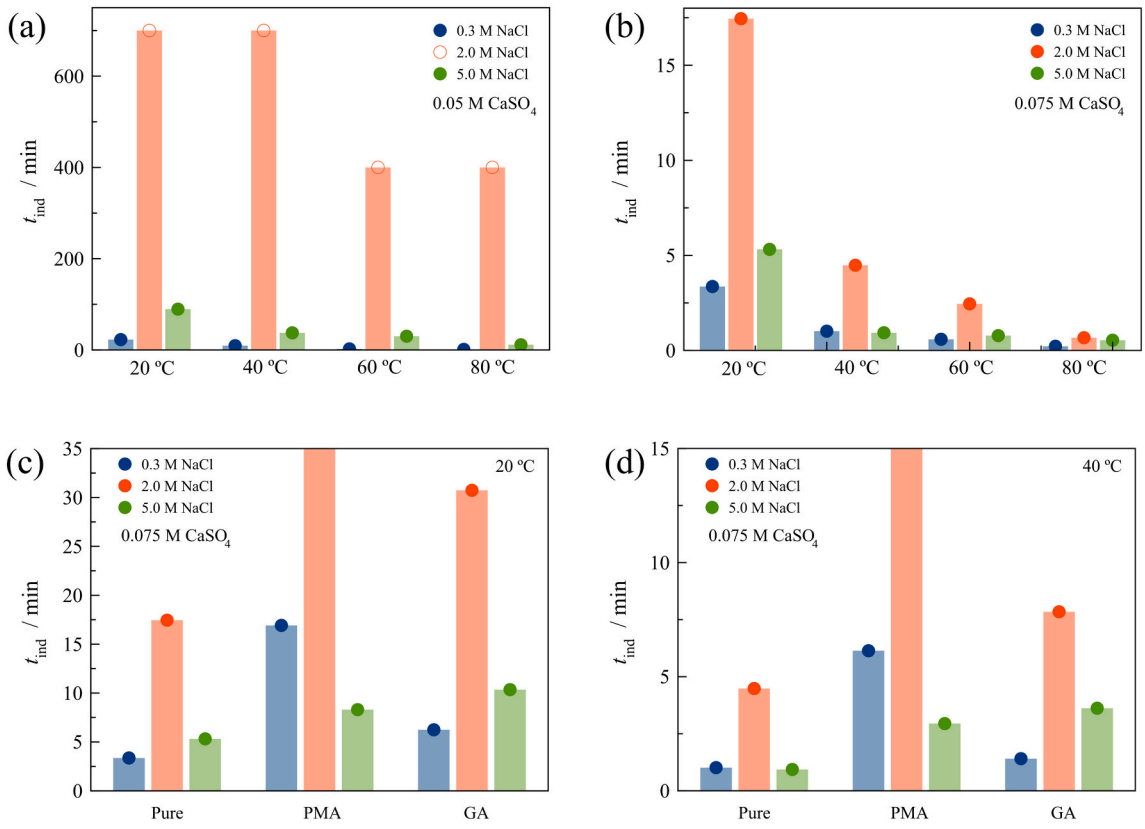

Fig. 8. Comparison of absolute induction times measured for calcium sulfate precipitation (a) 0.050 M and (b) 0.075 M $CaSO_4$ solutions at different temperatures and salinities without additives, and in 0.075 M $CaSO_4$ solutions containing (c) PM or (d) GA at different temperatures and background salinities. Open symbols in (a) indicate maximum observation times, after which no detectable precipitation had occurred. In (c), no precipitation was detected after 700 min in the presence of PM at 2 M NaCl and 20 °C, while nucleation occurred after 253 min under the same conditions at 40 °C in (d).

and less effective additives (cf. Fig. 4).

4. Concluding remarks and future work

In this work, we have developed a high-throughput benchtop method to rapidly determine the optimal operational window of ("green") antiscaling agents. This method was validated by (i) determining the scaling potential in the $CaSO_4$-NaCl-H_2O at different levels of supersaturation, temperatures and salinities, and (ii) characterizing the effects of two types of commonly used scale inhibitors, a chelating agent and a threshold inhibitor, during $CaSO_4$ precipitation across the same space of experimental conditions. Although the laboratory setup used for measuring induction times for scaling can probably not mimic the circumstances prevailing in industrial facilities such as desalination units, the results of these tests do provide direct and reliable information on the relative efficacy of the inhibitors because the experiments were all performed under identical conditions. To further demonstrate the generality of our methodology, we have tested different mineral systems and obtained viable results for the precipitation of CaCO3, BaSO4, SrSO4, Ca(OH)2, and CSH – as exemplified for barium sulfate nucleation in the presence of inhibiting and accelerating additives in Fig. S9. More comprehensive reports of the data collected for the various studied systems will be subject of forthcoming publications.

Aside from establishing the operational window for the two selected antiscaling agents, the experimental data collected in this work also highlights that adjusting the salinity of the solution can be an simple way to dramatically delay calcium sulfate precipitation even in the absence of any (polymeric) additive. Another interesting aspect revealed by the present results is the fact that the tested inhibitors display a quite different performance gradient as a function of solution conditions. In the case of the threshold inhibitor PM, we found that the strongest inhibiting action occurs at low supersaturation, low salinity and low to medium-high temperature, whereas no significant antiscaling effect was observed for PM in highly saline media. Based on these findings, we propose that PM exerts its inhibiting action by disrupting the initial formation and/or aggregation of primary $CaSO_4$ species (i.e. ions and/or ion clusters) and thus increasing the initial work required to form nuclei – interactions that may be screened once sufficiently high ionic strengths are reached. For, GA we observed a rather constant inhibiting potential – interesting for application in fluctuating operation conditions –, which is the result of the chelating of Ca^{2+} ions by GA.

Taken together, the method presented in this work allows for a rapid determination of scaling kinetics in a mineral system across a wide range of conditions, thus providing important information on the optimal operation window of antiscaling agents. This knowledge can likely be used to optimize antiscalant dosages in applied systems and consequently minimize the environmental impact. Simultaneously, the obtained data also shed new light on how additives manage to inhibit mineral precipitation, which will aid in the further development of next-generation additives with promising performance and sustainability profiles.

Abbreviation list

A	pre-exponential kinetic factor
CNT	classical nucleation theory
GA	D-gluconic acid
ICDD	International Centre for Diffraction Data
J	nucleation rate
k_B	Boltzmann constant

K_{sp}	solubility product
LC_0	maximum concentration causing no mortality
LD_{50}	lethal dose causing 50 % of mortality
$log_{10}S$	saturation index
M	molarity
MD	membranes during distillation
MW	molecular weight
PDF2	Powder Diffraction File - 2
PM	poly(methyl vinyl ether-*alt*-maleic acid)
ppm	parts per million
PXRD	powder X-ray diffraction
RO	reverse osmosis
S	saturation state
SI	supplementary information
SEM	scanning electron microscopy
T	temperature
t_{ind}	induction time
t_{pnc}	relaxation time to achieve a quasi-steady-state distribution of clusters
t_{nuc}	time elapsed to develop nuclei
t_{gr}	time required for the nuclei to grow to a detectable size
V	solution volume
W_*	work to form a critical cluster
γ_{eff}	effective interfacial free energy

CRediT authorship contribution statement

P. Ramírez-García: Investigation, Methodology, Formal analysis, Writing – original draft. **M.A. Duran-Olivencia:** Software, Methodology, Writing – review & editing. **M. Kellermeier:** Conceptualization, Writing – review & editing. **A.E.S. Van Driessche:** Conceptualization, Methodology, Supervision, Writing – review & editing, Funding acquisition.

Declaration of competing interest

The authors declare that they have no known competing financial interests or personal relationships that could have appeared to influence the work reported in this paper.

Data availability

Data will be made available on request.

Acknowledgements

This work was partially funded by Micro project 30.BA.94.0801 BIOTIC campus de excelencia (UGR).

Appendix A. Supplementary data

Supplementary data to this article can be found online at https://doi.org/10.1016/j.desal.2022.116128.

References

[1] Z. Amjad, K.D. Demadis (Eds.), Mineral Scales And Deposits: Scientific And Technological Applications, Elsevier, Amsterdam, 2015.
[2] D.M. Warsinger, J. Swaminathan, E. Guillen-Burrieza, H.A. Arafat, V.J.H. Lienhard, Scaling and fouling in membrane distillation for desalination applications: a review, Desalination 356 (2015) 294–313.
[3] A. Matin, F. Rahman, H.Z. Shafi, S.M. Zubair, Scaling of reverse osmosis membranes used in water desalination: phenomena, impact, and control; future directions, Desalination 455 (2019) 135–157.
[4] K.S.S. Christie, T. Horseman, R. Wang, C. Su, T. Tong, S. Lin, Gypsum scaling in membrane distillation: impacts of temperature and vapor flux, Desalination 525 (2022), 115499.
[5] V. Banakar, S.S. Sabnis, P.R. Gogate, A. Raha, A.K.Adak Saurabh, Comparison of sonocrystallization and seeding as pretreatment approaches for scale control to improve heat transfer in thermal brine concentrator, Desalination 523 (2022), 115444.
[6] A.A. Olajire, A review of oilfield mineral scale deposits management technology for oil and gas production, J. Pet. Sci. Eng. 135 (2015) 723–737.
[7] M. Mpelwal, S.F. Tang, State of the art of synthetic threshold scale inhibitors for mineral scaling in the petroleum industry: a review, Pet. Sci. 16 (2019) 830–849.
[8] T. Tong, A.F. Wallace, S. Zhao, Z. Wang, Mineral scaling in membrane desalination: mechanisms, mitigation strategies, and feasibility of scaling-resistant membranes, J. Membr. Sci. 579 (2019) 52–69.
[9] M. Bindels, J. Carvalho, C.B. Gonzalez, N. Brand, B. Nelemans, Techno-economic assessment of seawater reverse osmosis (SWRO) brine treatment with air gap membrane distillation (AGMD), Desalination 489 (2020), 114532.
[10] D. Hasson, H. Shemer, A. Sher, State of the art of friendly "green" scale control inhibitors: a review article, Ind. Eng. Chem. Res. 50 (2011) 7601–7607.
[11] D.A. Roberts, E.L. Johnston, N.A. Knott, Impacts of desalination plant discharges on the marine environment: a critical review of published studies, Water Res. 44 (2010) 5117.
[12] S. Kumar, T.K. Naiya, T. Kumar, Developments in oilfield scale handling towards green technology-a review, J. Pet. Sci. Eng. 169 (2018) 428–444.
[13] K.D. Demadis, Inorganic foulants in membrane systems: chemical control strategies and the contribution of "green chemistry", Desalination 179 (2005) 281–295.
[14] K. Popov, A. Boglovskiy, A. Gorbunov, O. Guseva, et al., A comparative study of phosphonate and phosphorus-free antiscalant efficiency by static and dynamic methods. Do we have reliable tools for an adequate reagent selection? Recent Adv. Petrochem. Sci. 1 (2017), 555557.
[15] O.S. Sannia, O. Bukuaghangin, T.V.J. Charpentier, A. Neville, Evaluation of laboratory techniques for assessing scale inhibition efficiency, J. Pet. Sci. Eng. 182 (2019), 106347.
[16] A.J. Karabelas, S.T. Mitrouli, M. Kostoglou, Scaling in reverse osmosis desalination plants: a perspective focusing on development of comprehensive simulation tools, Desalination 474 (2020), 114193.
[17] Y.A. Le Gouellec, M. Elimelech, Control of calcium sulfate (gypsum) scale in nanofiltration of saline agricultural drainage water, Environ. Eng. Sci. 19 (2002) 387–397.
[18] S.A. Ali, I.W. Kazi, F. Rahman, Synthesis and evaluation of phosphate-free antiscalants to control CaSO4·2H2O scale formation in reverse osmosis desalination plants, Desalination 357 (2015) 36–44.
[19] Z. Amjad, Gypsum scale formation on heated metal surfaces: the influence of polymer type and polymer stability on gypsum inhibition, Desalin. Water Treat. 51 (2013) 4709–4718.
[20] M. Schweinsberg, W. Hater, J. Verdes, New Stable Biodegradable Scale Inhibitor Formulations for Cooling Water: Development And Field Tests. Presented at the 64th International Water Conference, Pittsburgh, PA, Oct 19-23, 2003.
[21] A. Ketsetzi, A. Stathoulopoulou, K.D. Demadis, Being "Green" in chemical water treatment technologies: issues,challenges and developments, Desalination 223 (2008) 487.
[22] E. Elizondo, A. Córdoba, S. Sala, N. Ventosa, J. Veciana, Preparation of biodegradable poly (methyl vinyl ether-co-maleic anhydride) nanostructured microparticles by precipitation with a compressed antisolvent, J. Supercrit. Fluids 53 (2010) 108–114.
[23] A. Mira, C.R. Mateo, R. Mallavia, et al., Poly(methyl vinyl ether-alt-maleic acid) and ethyl monoester as building polymers for drug-loadable electrospun nanofibers, Sci. Rep. 7 (2017) 17205.
[24] T.W. Wong, S. Wahab, Y. Anthony, Effects of microwave on drug release property of poly(methyl vinyl ether-co-maleic acid) matrix, Drug Dev. Ind. Pharm. 33 (2007) 737–746.
[25] S. Ramachandran, et al., Gluconic acid: a review, Food Technol. Biotechnol. 44 (2006) 185–195.
[26] OECD , SIDS Initial Assessments Report for SIAM 18, Gluconic Acid, 526-95-4.
[27] F. Rahman, Calcium sulfate precipitation studies with scale inhibitors for reverse osmosis desalination, Desalination 319 (2013) 79–84.
[28] A. Rahardianto, W.-Y. Shih, R.-W. Lee, Y. Cohen, Diagnostic characterization of gypsum scale formation and control in RO membrane desalination of brackish water, J. Membr. Sci. 279 (2006) 655–668.
[29] M.Y. Ashfaq, M.A. Al-Ghouti, D.A. Da'na, H. Qiblawey, N. Zouari, Effect of concentration of calcium and sulfate ions on gypsum scaling of reverse osmosis membrane, mechanistic study, J. Mater. Res. Technol. 9 (2020) 13459–13473.
[30] M. Ossorio, A.E.S. Van Driessche, P. Perez, J.M. Garcia-Ruiz, The gypsum-anhydrite paradox revisited, Chem. Geol. 386 (2014) 16–21.
[31] S. Reigl, A.E.S. Van Driessche, J. Mehringer, S. Koltzenburg, W. Kunz, M. Kellermeier, Revisiting the roles of salinity, temperature and water activity in phase selection during calcium sulfate precipitation, CrystEngComm 24 (2022) 1529–1536.
[32] D.L. Parkhurst, C.A.J. Appelo, User's guide to PHREEQC - a computer program for speciation, reaction-path, 1D-transport, and inverse geochemical calculations, in: U.S. Geol. Survey Water Res. Invest. Rep 99, 1999, p. 4259.
[33] E. Giffaut, M. Grivé, P. Blanc, P. Vieillard, E. Colàs, H. Gailhanou, S. Gaboreau, N. Marty, B. Madé, L. Duro, Andra thermodynamic database for performance assessment: ThermoChimie, Appl. Geochem. 49 (2014) 225–236.
[34] J.W. Mullin, Crystallization, 4th Edition, Butterworth- Heinemann, Oxford, 2001.
[35] D. Kashchiev, G.M. van Rosmalen, Review: nucleation in solutions revisited, Cryst. Res. Technol. 38 (2003) 555–574.
[36] A.W. Nielsen, Kinetics of Precipitation, Pergamon, Oxford, 1964.
[37] T.M. Stawski, A.E.S. Van Driessche, M. Ossorio, J.D. Rodriguez-Blanco, R. Besselink, L.G. Benning, Formation of calcium sulfate through the aggregation of sub-3 nanometre primary species, Nat. Commun. 7 (2016) 11177.

[38] T.M. Stawski, R. Besselink, K. Chatzipanagis, J. Hovelmann, L.G. Benning, A.E. S. Van Driessche, Nucleation pathway of calcium sulfate hemihydrate (Bassanite) from solution: implications for calcium sulfates on Mars, J. Phys. Chem. C 124 (2020) 8411–8422.
[39] T. Yamazaki, et al., Two types of amorphous protein particles facilitate crystal nucleation, Proc. Natl. Acad. Sci. U. S. A. 114 (2017) 2154–2159.
[40] D. Kashchiev, Nucleation - Basic Theory With Applications, Butterworth-Heinemann, 2000.
[41] A.E.S. Van Driessche, M. Kellermeier, L.G. Benning, D. Gebauer, New Perspectives on Mineral Nucleation And Growth: From Solution Precursors to Solid Materials, 1st ed., Springer, New York, NY, 2017.
[42] A.E.S. Van Driessche, T.M. Stawski, M. Kellermeier, Calcium sulfate precipitation pathways in natural and engineered environments, Chem. Geol. 530 (2019), 119274.
[43] R Core Team, R: A Language And Environment for Statistical Computing, R Foundation for Statistical Computing, Vienna, Austria, 2020 https://www.R-project.org/.
[44] J.D. Martín-Ramos, Using XPowder: A Software Package for Powder X-ray Diffraction Analysis, 2004. D.L.GR-1001/04 (ISBN 84-609-1497-6).
[45] S. He, J.E. Oddo, M.B. Tomson, The nucleation kinetics of calcium sulfate dihydrate in NaCl solutions up to 6 m and 90 °C, J. Colloid Interface Sci. 162 (1994) 297–303.
[46] A. Lancia, D. Musmarra, M. Prisciandaro, Measuring induction period for calcium sulfate dihydrate precipitation, AICHE J. 45 (1999) 390–397.
[47] P.G. Klepetsanis, E. Dalas, P.G. Koutsoukos, Role of temperature in the spontaneous precipitation of calcium sulfate dihydrate, Langmuir 15 (1999) 1534–1540.
[48] A.E.S.Van Driessche, T.M. Stawski, L.G. Benning, M. Kellermeier, Calcium sulphate precipitation throughout its phase diagram, in: A.E.S. Van Driessche, M. Kellermeier, L.G. Benning, D. Gebauer (Eds.), New Perspectives on Mineral Nucleation And Growth, Springer-Verlag, Berlin/Heidelberg, 2017, pp. 227–256.
[49] C. Fan, A.T. Kan, G. Fu, M.S. Tomson, D. Shen, Quantitative evaluation of calcium sulfate precipitation kinetics in the presence and absence of scale inhibitors, Soc. Petrol. Eng. J. 15 (2010) 977–988.
[50] M. Prisciandaro, A. Lancia, D. Musmarra, Gypsum nucleation into sodium chloride solutions, AICHE J. 47 (2001) 929–934.
[51] H. Song, Y. Sun, F. Zhang, C.Z. Wang, K.M. Ho, M.I. Mendelev, Nucleation of stoichiometric compounds from liquid: role of the kinetic factor, Phys. Rev. Mater. 2 (2018), 023401.
[52] L. Nicoleau, A.E.S. Van Driessche, M. Kellermeier, A kinetic analysis of the role of polymers in mineral nucleation.The example of gypsum, Cem. Concr. Res. 124 (2019), 105837.
[53] D.T. Sawyer , Metal-Gluconate Complexes, Chem. Rev., 64 (61964) 633–643.
[54] M.C. van der Leeden, D. Kashchiev, G.M. van Rosmalen, Effect of additives on nucleation rate, crystal growth rate and induction time in precipitation, J. Cryst. Growth 130 (1993) 221–232.
[55] J. Vialetto, M. Anyfantakis, Exploiting additives for directing the adsorption and organization of colloid particles at fluid interfaces, Langmuir 37 (2021) 9302–9335.
[56] P. Denk, A. El Maangar, J. Lal, D. Kleber, T. Zemb, W. Kunz, Phase diagrams and microstructures of aqueous short alkyl chain polyethylene glycol ether carboxylate and carboxylic acid triblock surfactant solutions, J. Colloid Interface Sci. 15 (2021) 375–386.